Differential imprints of distinct ENSO flavors in global extreme precipitation patterns

Marc Wiedermann[1,2], **Jonatan F. Siegmund**[1,3], **Jonathan F. Donges**[1,4], **Jürgen Kurths**[1,2], **Reik V. Donner**[1]

[1]Potsdam Institute for Climate Impact Research — Telegrafenberg A 31, 14473 Potsdam, Germany, EU
[2]Department of Physics, Humboldt University — Newtonstraße 15, 12489 Berlin, Germany, EU
[3]Institute of Earth and Environmental Science, University of Potsdam, Karl-Liebknecht-Straße 24-25, 14476 Potsdam-Golm, Germany
[4]Stockholm Resilience Centre, Stockholm University — Kräftriket 2B, 114 19 Stockholm, Sweden, EU

arXiv:1702.00218v1 [physics.ao-ph] 1 Feb 2017

Key Points:

- Global assessment of ENSO related impacts on seasonal precipitation extremes
- East Pacific El Niños and La Niñas trigger spatially coherent extreme precipitation responses
- Central Pacific events result in less spatially coherent precipitation extremes

Corresponding author: Marc Wiedermann, marcwie@pik-potsdam.de

Abstract
The specific impacts of El Niño's two flavors, East Pacific (EP) and Central Pacific (CP) El Niño, have been studied intensively in recent years, mostly by applying linear statistical or composite analyses. These techniques, however, focus on average spatio-temporal patterns of climate variability and do not allow for a specific assessment of related extreme impacts. Here, we use event coincidence analysis to study the differential imprints of EP and CP types of both, El Niño and La Niña on global extreme precipitation patterns. We provide a detailed statistical assessment of seasonal precipitation extremes related to the two flavors of both phases of the El Niño Southern Oscillation (ENSO) in terms of their likelihood and spatial extent. Our analysis recaptures previously reported interrelations and uncovers further regional extremes arising along with different ENSO phases that have not been reported so far.

1 Introduction

The El Niño Southern Oscillation (ENSO) with its positive (El Niño) and negative phase (La Niña) is known to trigger climatic responses in various parts of the Earth, an effect that is often referred to as teleconnectivity [*Trenberth*, 1997; *Neelin et al.*, 2003]. Specifically, it has been observed in recent years that El Niño further exhibits two distinct types, usually referred to as the East Pacific or canonical El Niño and the Central Pacific El Niño or El Niño Modoki, respectively [*Ashok et al.*, 2007; *Kao and Yu*, 2009]. A similar proposition regarding the existence of two distinct flavors was made recently for La Niña as well [*Kug and Ham*, 2011], but is a subject of ongoing studies [*Kao and Yu*, 2009; *Ren and Jin*, 2011]. For El Niño, it has been shown that its two types may cause different climatic responses in certain regions, such as reduced rainfall over eastern Australia during EP El Niños [*Chiew et al.*, 1998] contrasted by an increase in precipitation over the same area during CP El Niños [*Taschetto and England*, 2009].

Most previous studies on El Niño's teleconnective impacts have either applied linear statistical tools, such as correlation analysis [*Diaz et al.*, 2001], or investigated corresponding composites of the climatic observables under study [*Hoell et al.*, 2014]. Both approaches share the limitation that they focus on linear or average interdependencies between ENSO and possible response variables, which do not necessarily hold for extreme values. However, with global climate change projected to increase the strength and frequency of both, extreme climatic events [*Jones et al.*, 2007; *Karl and Trenberth*, 2003; *Easterling et al.*, 2000] as well as extreme ENSO periods [*Cai et al.*, 2014] it has become a pressing issue to specifically assess possible linkages between these two aspects [*Allan and Soden*, 2008]. Therefore, we devote the present work to quantify and spatially resolve signatures of extreme climatic events that are likely to coincide with an ENSO phase of a certain type. In particular, we focus here on heavy precipitation and dry periods, i.e., hydro-meterological extreme events, as ENSO has been shown to largely affect rainfall patterns at both global and regional scales [*Dai and Wigley*, 2000; *Ropelewski and Halpert*, 1987].

The main goal of this study is to quantify the likelihood of simultaneous or time-delayed occurrences of localized precipitation extremes along with an ENSO phase of a given type. For this purpose, we employ *event coincidence analysis* (ECA) [*Donges et al.*, 2011, 2016] for estimating the probability of co-occurrences between such events. This framework has already been successfully applied to quantifying the likelihood of climatic extreme events triggering certain ecological or social responses, such as extreme annual [*Rammig et al.*, 2015] and daily [*Siegmund et al.*, 2016a] tree growth or flowering dates [*Siegmund et al.*, 2016b] as well as the outbreak of epidemics [*Donges et al.*, 2016] or violent conflicts [*Schleussner et al.*, 2016]. Acknowledging the already observed differential impacts of EP and CP El Niños, we aim here to further characterize specific extreme impacts of the two flavors of both, El Niño and La Niña.

Several schemes to distinguish EP from CP events have been proposed in the recent past. One prominent example is the *ENSO Modoki Index* that is computed as the weighted average sea surface temperature in the equatorial Pacific [*Ashok et al.*, 2007]. Other studies used em-

pirical orthogonal functions [*Graf and Zanchettin*, 2012; *Kao and Yu*, 2009] or combinations of the Nino3 and Nino4 indices [*Kim et al.*, 2011; *Hu et al.*, 2011] to provide the desired discriminations. In contrast to statistics related solely to the dynamics within the equatorial Pacific, *Wiedermann et al.* [2016] recently introduced an index to discriminate different ENSO flavors based on the assessment of global teleconnections in surface air temperature. This index shows a more distinct and sharp discrimination as compared to previously proposed measures based on average temperature observations [*Ashok et al.*, 2007]. This particular property is important for our present analysis as ECA relies on the assessment of event sequences, which are easily computed for a spike-like signal in contrast to a smoothly varying one.

We use the index proposed by *Wiedermann et al.* [2016] together with the classical Oceanic Nino Index (ONI) (provided by the Climate Prediction Center of the National Oceanic and Atmospheric Administration, NOAA-CPC) to construct four event series representing EP and CP El Niño and La Niña phases. We then utilize ECA to quantify simultaneous occurrences of either of the four ENSO types with spatially resolved seasonal precipitation extremes (wet and dry) in boreal fall and winter of the same year as the start of a certain ENSO episode, and spring of the following year. The data and methods applied in this work are presented in Sec. 2. Section 3 shows the results of our analysis. We start by evaluating the effects of the canonical El Niño on extreme precipitation and demonstrate the validity of our approach by comparing the obtained spatial patterns with recent studies. We then focus on CP El Niños and highlight differences with their EP counterparts. Ultimately, we study La Niña periods and show that most extreme rainfall responses are attributed to the EP type of ENSO's negative phase. We thus conclude that in the light of recent discussions on the existence of two types of La Niña [*Kug and Ham*, 2011] it is meaningful to distinguish one type that significantly affects global precipitation signals and one that shows hardly any spatially coherent impact. Finally, Sec. 4 provides the conclusions of this work as well as suggestions for future research.

2 Data & Methods

2.1 GPCC rainfall data

We utilize gridded monthly precipitation data provided by the Global Precipitation Climatology Centre (GPCC) at a spatial resolution of 2.5°×2.5° [*Schneider et al.*, 2015]. Since reliable estimations of El Niño and La Niña periods according to the ONI as well as a discrimination into their respective EP and CP flavors are only available for the second half of the 20th century so far, we restrict our analysis to the period from 1951 to 2015. Note that the density of stations from which the data is derived varies between 0 and more than 100 per grid cell and for different years [*Lorenz and Kunstmann*, 2012], which generally results in a lower accuracy and reliability of the data for those areas with only few stations [*Rudolf et al.*, 1994]. We therefore consider only grid cells where the average number of stations between 1951 and 2010 is larger than 1, yielding a total number of $N = 2248$ cells. From the monthly time series, we derive separate records for three seasons s by aggregating the precipitation amounts of the corresponding three-month periods September to November (SON), December to February (DJF) and March to May (MAM). This results in three time series $P_{i,s}(t)$ per grid cell i with $M = 62$ annual values each.

2.2 Network transitivity index of ENSO flavor

Previous approaches to distinguish different flavors of El Niño [*Hendon et al.*, 2009] like empirical orthogonal function (EOF) analysis [*Graf and Zanchettin*, 2012] or the ENSO Modoki Index (EMI) [*Ashok et al.*, 2007] often yielded ambiguous or mutually inconsistent results [*Wiedermann et al.*, 2016]. *Radebach et al.* [2013] were the first to observe that characteristics related to the global correlation structure of surface air temperatures expressed as a complex net-

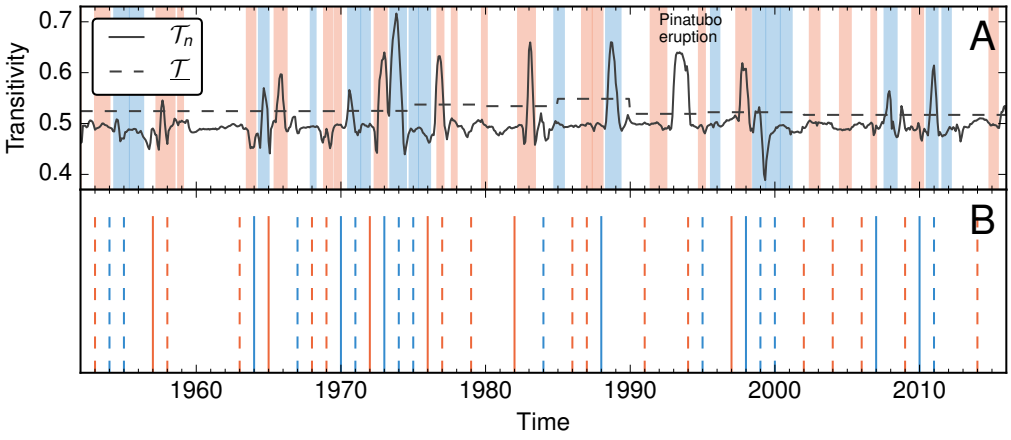

Figure 1. (A) Network transitivity index indicating EP El Niños or La Niñas if its value exceeds the baseline (dashed line), and CP phases otherwise. Red and blue shaded areas indicate periods of El Niño and La Niña according to the ONI. (B) Corresponding series of EP (solid) and CP (dashed) El Niño (red) and La Niña (blue) events, respectively.

work can provide sharp discriminators between EP and CP El Niños. Inspired by this approach, *Wiedermann et al.* [2016] recently developed an index based on climate network transitivity $\mathcal{T}$, a measure to quantify the degree of localization of ENSO's global teleconnections, displaying different spatial characteristics for EP and CP flavors of El Niño and La Niña.

The transitivity index is computed upon daily global surface air temperature anomalies (SATA) from the NCEP/NCAR reanalysis [*Kistler et al.*, 2001] used to construct a sequence of 365-days long running-window cross-correlation matrices $\mathbf{C}_n = (C_{n,ij})$ between all pairs of time series in the data set. The most relevant information captured by C_n is contained in the 0.5% of strongest absolute correlations for each window n and expressed using thresholds T_n such that

$$W_{n,ij} = |C_{n,ij}| \cdot \Theta(|C_{n,ij}| - T_n), \tag{1}$$

with $\Theta(\cdot)$ denoting the Heaviside function. One major characteristic of the resulting matrix W_n is the transitivity index

$$\mathcal{T}_n = \frac{\sum_{i,j,k} w_i W_{n,ij} w_j W_{n,jk} w_k W_{n,ki}}{\sum_{i,j,k} w_i W_{n,ij} w_j W_{n,jk} w_k} \in [0,1] \tag{2}$$

with

$$w_i = \cos(\lambda_i). \tag{3}$$

Here, λ_i denotes the latitudinal position of each time series' corresponding grid point on the Earth's surface [*Heitzig et al.*, 2012; *Tsonis et al.*, 2006]. A comprehensive description of the above framework is given in *Wiedermann et al.* [2016].

Figure 1A shows the temporal evolution of the transitivity index. In contrast to the EMI, it provides a sharp and distinct discrimination between the two El Niño flavors (and also two corresponding types of La Niña phases), such that a peak in the index indicates an EP type while its absence points to a CP event. A corresponding baseline $\underline{\mathcal{T}}$ (dashed horizontal line in Fig. 1A) above which values of $\mathcal{T}$ are considered a peak is given as well. It is derived as the transitivity computed over the same 30-year periods that are used to determine the base periods for the computation of sea surface temperature anomalies in the definition of the ONI.

2.3 Data preprocessing

We define years with seasons s (DJF, SON, or MAM, see Sec. 2.1) exhibiting extraordinary high or low precipitation amounts from the corresponding time series $P_{s,i}(t)$ for each grid cell i, individually. Specifically, we consider values above (below) the 80th (20th) percentile $p^{+}_{s,i}$ ($p^{-}_{s,i}$) in each of the time series $P_{s,i}(t)$ as extraordinary high (low) seasonal precipitation sums. We choose these particular thresholds to ensure the presence of a sufficient number of particularly dry and wet seasons that is comparable with the number of different ENSO phases in the considered time period. It has been checked that the results obtained in the following do not change qualitatively if more restrictive thresholds are applied (not shown).

According to these considerations, we obtain six binary time series $P^{\pm}_{s,i}(t)$ per grid cell,

$$P^{\pm}_{s,i}(t) = \Theta(\pm P_{s,i}(t) \mp p^{\pm}_{s,i}), \tag{4}$$

where $P^{\pm}_{s,i}(t) = 1$ indicates the presence of a seasonal precipitation extreme at grid cell i during season s in year t. By following the above procedure, no further de-seasonalisation of the precipitation data is necessary, since the grid cell-specific seasonality of precipitation is already taken into account. Furthermore, the events are defined for each location independent from the others and therefore spatial heterogeneity is taken into account as well.

In addition to the precipitation data set, we create similar binary indicator time series for the different ENSO phases (Fig. 1B), e.g. an EP El Niño series $X_{EPEN}(t)$ with $X_{EPEN} = 1$ if t marks the onset year of an El Niño period (as defined by the ONI) and $\mathcal{T}_n$ exceeds $\underline{\mathcal{T}}$ for at least one month of that considered period. All remaining El Niño periods are classified as CP events, yielding a corresponding event series $X_{CPEN}(t)$ (solid and dashed red lines in Fig. 1B). The same procedure is applied to La Niña periods, yielding event series $X_{EPLN}(t)$ and $X_{CPLN}(t)$, respectively (blue lines in Fig. 1B).

2.4 Event Coincidence Analysis

We apply event coincidence analysis (ECA), a statistical tool to quantify simultaneities between events in two series [*Donges et al.*, 2011; *Rammig et al.*, 2015; *Donges et al.*, 2016]. It computes for each grid cell the fraction of EP (CP) El Niño (La Niña) phases that coincide with extreme precipitation sums in SON or DJF of the same year or MAM of the following year, revealing if the timing of precipitation extremes is non-randomly related to the presence of a given type of ENSO phase. Specifically, the event coincidence rate $ECR^{\pm}_{s,i,\bullet}$ for one pair of ENSO and precipitation event series is given by

$$ECR^{\pm}_{s,i,\bullet} = \frac{\sum_t X_\bullet(t) P\pm_{s,i}(t-\tau)}{\sum_t X_\bullet(t)}. \tag{5}$$

Here, $X_\bullet(t)$ represents one of the four time series indicating EP and CP types of El Niño and La Niña. The offset τ reads $\tau = 0$ for SON and DJF and $\tau = 1$ for MAM.

To assess the statistical significance of the obtained event coincidence rates, we assume both involved event sequences to be distributed randomly, independently and uniformly [*Donges et al.*, 2011; *Rammig et al.*, 2015; *Siegmund et al.*, 2016b,a]. A corresponding p-value is estimated analytically from the (binomial) probability distribution of event coincidence rates that would occur by chance only. We consider an empirical event coincidence rate as statistically significant if its p-value is smaller than a confidence level of $\alpha = 0.05$ (for mathematical details, see *Donges et al.* [2016]).

3 Results & Discussion

3.1 Seasonal precipitation extremes and EP El Niño

We first investigate event coincidences rates between EP El Niños and the timing of seasonal precipitation extremes. Figures 2A,C,E show locations with significant coincidence rates

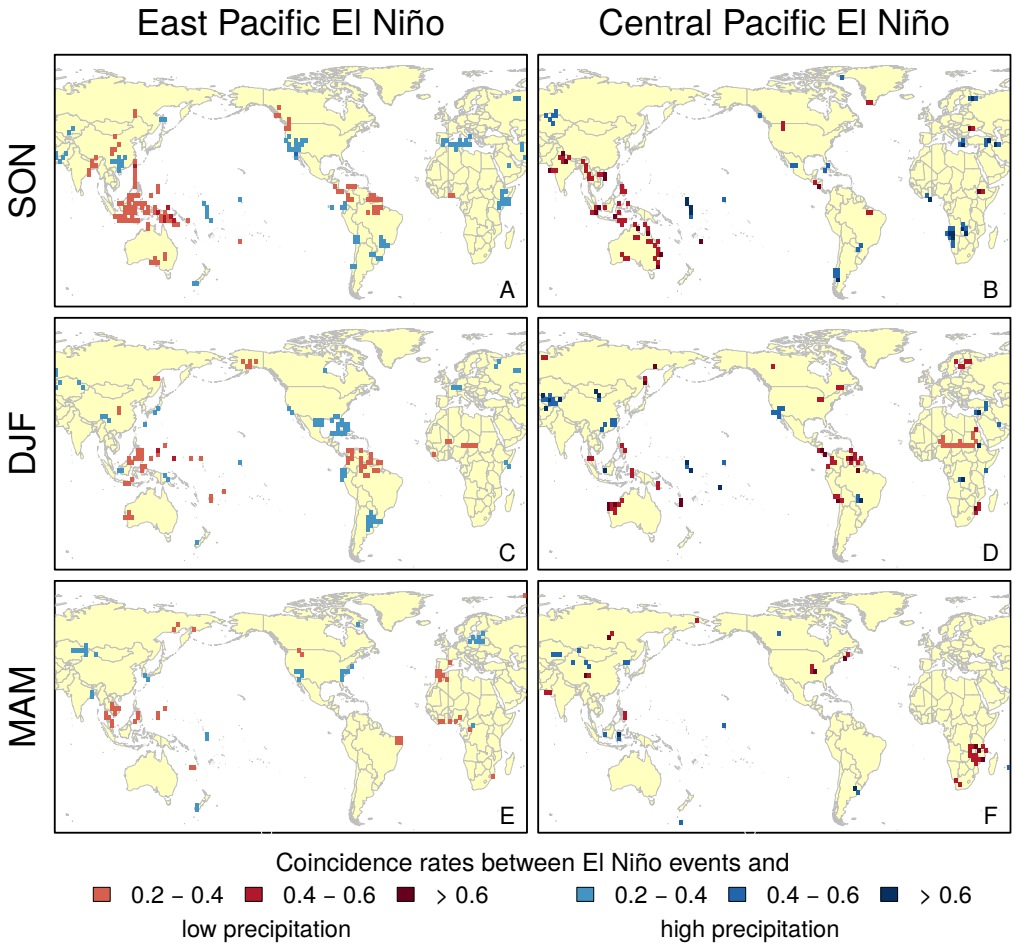

Figure 2. Statistically significant event coincidence rates between years of EP (left column) and CP (right column) El Niños and very dry or very wet seasons (SON, DJF, MAM). Red (blue) squares represent grid cells with significant event coincidence rates between EP or CP El Niño years and seasonal precipitation sums below (above) the 20th (80th) percentile of all years from 1951 to 2015.

$ECR^{\pm}_{\bullet,i,ENEP}$ between EP El Niños and extremely dry (red squares) and wet periods (blue squares) in SON, DJF and MAM, respectively.

During SON of EP El Niño years, we find an elevated probability of extremely dry conditions over Indonesia, the Philippines and the southwestern Pacific islands as well as over northern South America and the northern Amazon Basin (Fig. 2A). For the same season, we also observe an increased likelihood of very wet conditions over the central Pacific islands and the west coast of North America. (Fig. 2A). Similarly wet conditions are found over Ecuador and the South American east coast in SON and DJF (Fig. 2A,B). All these observations agree well with previous studies [e.g. *Diaz et al.*, 2001]. Coinciding with EP El Niños, we also observe more frequent wet extremes over the Mediterranean region (Fig. 2A) in SON, which was partially also reported earlier by *Shaman and Tziperman* [2010]. Furthermore, the wet conditions over East Africa during the same season (Fig. 2A) have previously been described in parts by *Camberlin et al.* [2001]. Finally, we observe very dry conditions in southwestern Africa during DJF (Fig. 2C) as also reported by *Hoell et al.* [2014].

Generally, our ECA results are in good agreement with previously reported interrelations between El Niño and global precipitation, which have mostly been identified using linear cor-

relation analysis. Thus, we conclude that (i) the application of ECA to assess ENSO-related extreme impacts provides valid results, and that (ii) extreme responses to the canonical El Niño display roughly similar spatial patterns as the average statistical interdependency between ENSO-related indices and climatic observables. However, we note that most previous studies have not discriminated between the two El Niño flavors. Thus, the agreement between our results for EP El Niños and the recent literature suggests that the previously observed linear effects might just be dominated by the (on average stronger) EP events.

3.2 Seasonal precipitation extremes and CP El Niño

Next, we focus on the specific effects of the less intensively studied CP El Niño and estimate event coincidence rates between these phases and seasons with extreme precipitation sums (Fig. 2B,D,E). We first discuss those regions that display significant coincidence rates for EP El Niños (see Sec. 3.1) but an absence or altered likelihood of precipitation extremes during CP periods. Notably, the dry events over Central America and the Amazon that frequently occur together with EP El Niños become more likely during DJF (Fig. 2D) but show insignificant coincidence rates in SON (Fig,. 2B). The latter also holds for the wet events along the western coast of Central and North America that have been observed for EP El Niños. In the same manner, the wet SON patterns over Southern China, the Mediterranean, and South-East Africa coinciding with EP El Niños disappear during CP events (Fig,. 2B). We further note, that the large-scale dry events over Indonesia observed along with EP events during SON become less spatially coherent for CP El Niños (Fig. 2B). For MAM, the wet and dry patterns over Europe become insignificant (Fig. 2F).

While the above observations indicate decreased or weakened impacts of CP El Niños in comparison with the EP type, we also observe the emergence of new patterns that are not present during EP El Niños but emerge only along with CP phases. Specifically, dry events become more likely along Australia's east coast during SON (Fig. 2B), and significant coincidence rates with wet events arise over the south of Chile pointing towards increased rainfall during CP El Niños as compared to their canonical counterparts. In DJF months coinciding with CP events, we observe the emergence of new wet patterns over Central Asia and China as well as a dry pattern over the north of Chile (Fig. 2D). Ultimately, for MAM we observe a pronounced dry pattern over Southeast Africa (Fig. 2F). Generally, we note a decrease in the spatial coherence of seasonal precipitation extremes coinciding with CP El Niños in comparison with EP phases.

3.3 Seasonal precipitation extremes and EP/CP La Niña

We finally perform the same analysis for La Niña periods. For the EP, i.e. canonical, La Niña type (Fig. 3A,C,E) we again find various patterns that were reported in earlier studies. Specifically, during SON coinciding with EP La Niña phases (Fig. 3A) we find the expected wet conditions over Australia and Indonesia [*Arblaster et al.*, 2002] and exceptionally dry conditions in parts of southern Europe [*Pozo-Vázquez et al.*, 2005] and the south of Brazil [*Ropelewski and Halpert*, 1996]. We further observe significant coincidence rates with dry events in the middle East and with extreme rainfall over central Europe. For DJF, our analysis confirms findings by *Nicholson and Selato* [2000] of wet conditions over South Africa and dry events over West Africa (Fig. 3C). We further observe a prominent extreme precipitation dipole with dry conditions over Mexico and increased rainfall in the southwestern part of Canada. For MAM seasons associated with EP La Niñas, we observe a tendency towards extreme rainfall over the Amazon [*Rogers*, 1988] and parts of Northern Australia [*Arblaster et al.*, 2002] (Fig. 3).

In contrast to the coherent patterns observed for EP La Niña phases, we find only a few spatially organized structures during CP events (Fig. 3B, E, F). Most prominently, we recover previously reported wet conditions over parts of Australia in DJF [*Arblaster et al.*, 2002; *Cai and Cowan*, 2009] (Fig. 3B). Additionally, we uncover strongly reduced rainfall over Florida in DJF, and over Scandinavia and the south of Russia in MAM. Thus, similar as for El Niño,

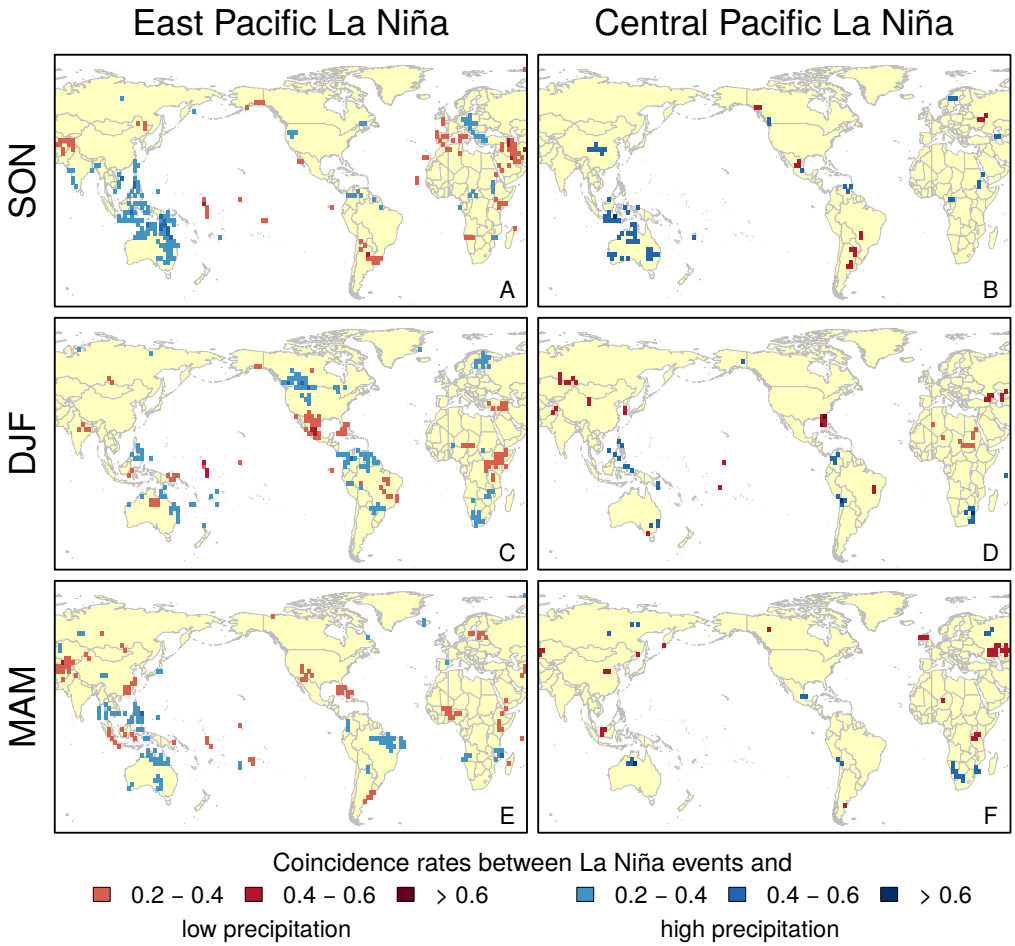

Figure 3. Same as Fig. 2 for La Niña periods.

we again observe that CP La Niñas coincide with less spatially coherent extreme precipitation responses.

Following upon the presented findings, we pick up the recently raised question whether it is actually meaningful to distinguish La Niña into two flavors in the same fashion as El Niño [*Kug and Ham*, 2011]. While *Kao and Yu* [2009] and *Ashok and Yamagata* [2009] advocated for such a distinction, *Kug et al.* [2009] and *Ren and Jin* [2011] argued that based on correlation analyses between La Niña related SST patterns no distinct discrimination into two types is evident. Contributing to this discussion, *Wiedermann et al.* [2016] demonstrated that according to the transitivity index characterizing ENSO teleconnectivity it is indeed meaningful to provide a discrimination of La Niño periods analogous to El Niño. The results of our current work demonstrate that seasonal precipitation extremes accompanied by EP La Niñas are generally more likely to arise in a spatially coherent way (Fig. 3) than such observed along with CP phases. The same property also holds for El Niño periods (Sec. 3.2), which highlights again a symmetry not only within the spatial patterns of El Niño and La Niña themselves, but also with respect to their induced extreme precipitation responses. Thus, from an impact-oriented point of view, our work provides further evidence in favor of a distinction between two types of La Niña indicated by the presence or absence of induced seasonal precipitation extremes. In other words, from the viewpoint of extreme events (and thus possibly in contrast to observations based on linear statistical analysis) it seems reasonable to discriminate La Niña into two types in the same way as for El Niño periods.

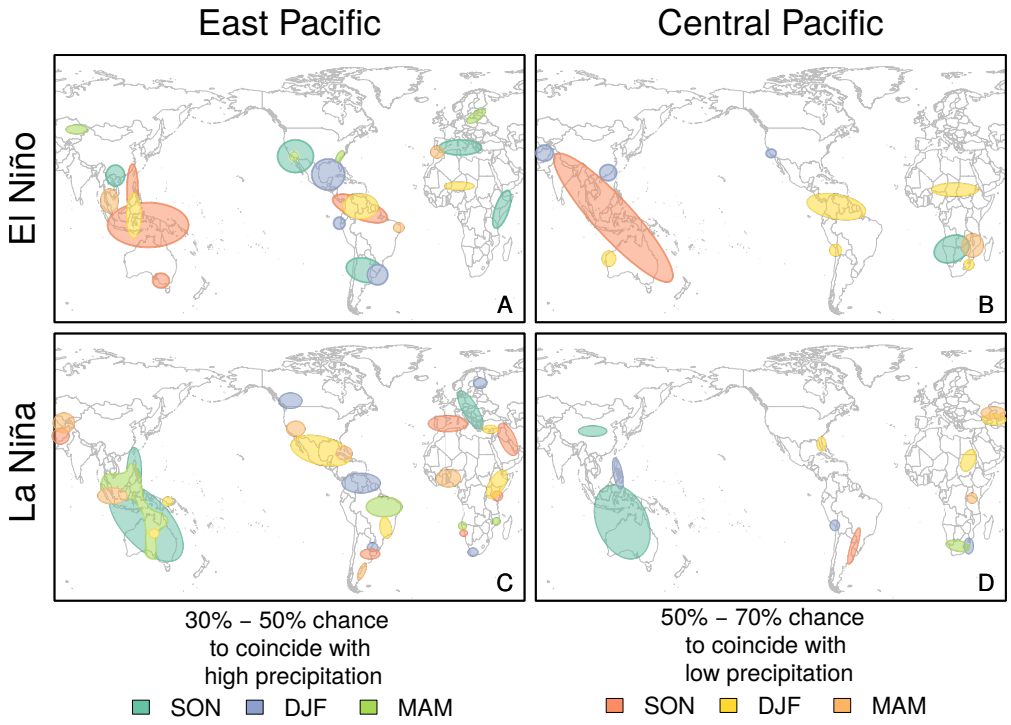

Figure 4. Schematic summary of the results of this work. Shaded areas indicate geographic locations for which extreme (high or low) seasonal precipitation sums exhibit significant coincidence rates with EP (A,C) or EP (B,D) El Niño (A,B) or La Niña phases (C,D). For all indicated areas related to EP (CP) phases, seasonal precipitation extremes occur with a probability of 30-50% (50-70%), respectively.

4 Conclusion & Outlook

We have carried out a detailed analysis of ENSO imprints in global patterns of seasonal precipitation extremes. Specifically, we discriminated both, El Niño and La Niña into two distinct types (East Pacific and Central Pacific) by utilizing the network transitivity index $\mathcal{T}$ introduced by *Wiedermann et al.* [2016]. From $\mathcal{T}$, four distinct event series were defined such that an event in each series corresponds to the presence of the respective type of ENSO event. The globally gridded GPCC rainfall data set was aggregated to grid point-wise seasonal precipitation sums, and corresponding event series were obtained by applying the 80th (20th) percentile to define extremely wet (dry) periods.

We then used event coincidence analysis [*Siegmund et al.*, 2016a; *Donges et al.*, 2016] to identify grid points with significant coincidence rates between different types of ENSO phases and seasonal precipitation extremes. Our analysis confirmed that previously observed interrelationships based on linear correlation or composite analysis also apply to the associated extremes. In addition, we identified further impacts of ENSO episodes, especially of the Central Pacific types of both, El Niño and La Niña, which have to our current knowledge not been described so far. This implies that in these cases, classical analysis methods may not be sufficienct to capture such interrelations. Moreover, it shows that even though a general linear relationship between ENSO and precipitation might be weak or absent for a given region, dry periods or heavy rainfall can still be possible effects of specific types of ENSO phases. At the same time we observe that most previously observed interrelations only hold for events corresponding to East Pacific ENSO flavors. This implies that with a proper discrimination of event types, threats like possible droughts or flooding can be better anticipated, since for most re-

gions of the Earth, CP types of ENSO events have no or a less spatially organized impact on seasonal precipitation extremes.

Our analysis contributed to the ongoing discourse whether or not it is (statistically and climatologically) meaningful to discriminate La Niña into two flavors in the same way as done for El Niño. The obtained results suggest that such congruence between ENSO's positive and negative phase is meaningful in both ways as (i) the transitivity index clearly distinguishes between two types of events for El Niño as well as La Niña and (ii) event coincidence analysis shows that the EP La Niña displays more spatially coherent seasonal precipitation extremes, while fewer impacts are found for its Central Pacific counterpart.

In conclusion, our analysis provided a detailed and global overview on the large-scale imprints of different ENSO phases and flavors in extreme seasonal precipitation patterns. All findings are ultimately summarized in Fig. 4, which displays schematically all regions for which the four different types of ENSO phases show significant coincidence rates with seasonal precipitation extremes together with these rates.

Future work shall apply the concepts used in this work to also study ENSO related extreme impacts on further climatic observables, such as temperature. Also, a more thorough intercomparison between results obtained from linear and event statistics could prove useful in assessing which regions are most affected in terms of extreme climatic responses to the presence of either type and phase of ENSO. Ultimately, it could be useful to apply the presented framework also to future climate projections in order to assess possible changes in spatial extent and frequency of ENSO related extreme events.

Acknowledgments

MW, JFS and RVD acknowledge funding by the German Federal Ministry for Education and Research (BMBF) via the Young Investigators Group CoSy-CC^2 (grant no. 01LN1306A). JFD thanks the Stordalen Foundation and the Leibniz Society (project DOMINOES) for financial support. JK and RVD acknowledge the IRTG 1740 funded by DFG and FAPESP. JFS has been supported by the Evangelisches Studienwerk Villigst e.V. All computations have been performed using the R package `CoinCalc` [*Siegmund et al.*, 2017].

References

Allan, R. P., and B. J. Soden (2008), Atmospheric Warming and the Amplification of Precipitation Extremes, *Science*, *321*(5895), 1481–1484, doi:10.1126/science.1160787.

Arblaster, J., G. Meehl, and A. Moore (2002), Interdecadal modulation of Australian rainfall, *Clim. Dynam.*, *18*(6), 519–531, doi:10.1007/s00382-001-0191-y.

Ashok, K., and T. Yamagata (2009), Climate change: The El Niño with a difference, *Nature*, *461*(7263), 481–484, doi:10.1038/461481a.

Ashok, K., S. K. Behera, S. A. Rao, H. Weng, and T. Yamagata (2007), El Niño Modoki and its possible teleconnection, *J. Geophys. Res.*, *112*(C11), C11,007, doi:10.1029/2006JC003798.

Cai, W., and T. Cowan (2009), La Niña Modoki impacts Australia autumn rainfall variability, *Geophys. Res. Lett.*, *36*(12), L12,805, doi:10.1029/2009GL037885.

Cai, W., S. Borlace, M. Lengaigne, P. van Rensch, M. Collins, G. Vecchi, A. Timmermann, A. Santoso, M. J. McPhaden, L. Wu, M. H. England, G. Wang, E. Guilyardi, and F.-F. Jin (2014), Increasing frequency of extreme El Niño events due to greenhouse warming, *Nature Clim. Change*, *4*(2), 111–116, doi:10.1038/nclimate2100.

Camberlin, P., S. Janicot, and I. Poccard (2001), Seasonality and atmospheric dynamics of the teleconnection between African rainfall and tropical sea-surface temperature: Atlantic vs. ENSO, *Int. J. Climatol.*, *21*(8), 973–1005, doi:10.1002/joc.673, wOS:000169831700004.

Chiew, F. H. S., T. C. Piechota, J. A. Dracup, and T. A. McMahon (1998), El Niño/Southern Oscillation and Australian rainfall, streamflow and drought: Links and potential for forecasting, *J. Hydrol.*, *204*(14), 138–149, doi:10.1016/S0022-1694(97)00121-2.

Dai, A., and T. M. L. Wigley (2000), Global patterns of ENSO-induced precipitation, *Geophys. Res. Lett.*, *27*(9), 1283–1286, doi:10.1029/1999GL011140.

Diaz, H. F., M. P. Hoerling, and J. K. Eischeid (2001), ENSO variability, teleconnections and climate change, *Int. J. Climatol.*, *21*(15), 1845–1862, doi:10.1002/joc.631.

Donges, J. F., R. V. Donner, M. H. Trauth, N. Marwan, H.-J. Schellnhuber, and J. Kurths (2011), Nonlinear detection of paleoclimate-variability transitions possibly related to human evolution, *P. Natl. Acad. Sci.*, *108*(51), 20,422–20,427, doi:10.1073/pnas.1117052108.

Donges, J. F., C.-F. Schleussner, J. F. Siegmund, and R. V. Donner (2016), Event coincidence analysis for quantifying statistical interrelationships between event time series: on the role of flood events as triggers of epidemic outbreaks, *Eur. Phys. J. S. T.*, *225*(3), 471–487, doi:10.1140/epjst/e2015-50233-y.

Easterling, D. R., J. Evans, P. Y. Groisman, T. Karl, et al. (2000), Observed variability and trends in extreme climate events: a brief review, *Bull. Amer. Meteor. Soc.*, *81*(3), 417.

Graf, H.-F., and D. Zanchettin (2012), Central Pacific El Niño, the subtropical bridge, and Eurasian climate, *J. Geophys. Res.*, *117*(D1), doi:10.1029/2011JD016493.

Heitzig, J., J. F. Donges, Y. Zou, N. Marwan, and J. Kurths (2012), Node-weighted measures for complex networks with spatially embedded, sampled, or differently sized nodes, *Eur. Phys. J. B*, *85*(1), 1–22, doi:10.1140/epjb/e2011-20678-7.

Hendon, H. H., E. Lim, G. Wang, O. Alves, and D. Hudson (2009), Prospects for predicting two flavors of El Niño, *Geophys. Res. Lett.*, *36*(19), L19,713, doi:10.1029/2009GL040100.

Hoell, A., C. Funk, T. Magadzire, J. Zinke, and G. Husak (2014), El Niño-Southern Oscillation diversity and Southern Africa teleconnections during Austral Summer, *Clim. Dynam.*, *45*(5-6), 1583–1599, doi:10.1007/s00382-014-2414-z.

Hu, Z.-Z., A. Kumar, B. Jha, W. Wang, B. Huang, and B. Huang (2011), An analysis of warm pool and cold tongue El Niños: air-sea coupling processes, global influences, and recent trends, *Clim. Dynam.*, *38*(9-10), 2017–2035, doi:10.1007/s00382-011-1224-9.

Jones, P., K. Trenberth, P. Ambenje, R. Bojariu, D. Easterling, T. Klein, D. Parker, J. Renwick, M. Rusticucci, B. Soden, et al. (2007), Observations: surface and atmospheric climate change, *Climate change 2007: the physical science basis. Contribution of Working Group I to the Fourth Assessment Report of the Intergovernmental Panel on Climate Change*, pp. 235–336.

Kao, H.-Y., and J.-Y. Yu (2009), Contrasting Eastern-Pacific and Central-Pacific Types of ENSO, *J. Climate*, *22*(3), 615–632, doi:10.1175/2008JCLI2309.1.

Karl, T. R., and K. E. Trenberth (2003), Modern global climate change, *Science*, *302*(5651), 1719–1723.

Kim, W., S.-W. Yeh, J.-H. Kim, J.-S. Kug, and M. Kwon (2011), The unique 2009-2010 El Niño event: A fast phase transition of warm pool El Niño to La Niña, *Geophys. Res. Lett.*, *38*(15), L15,809, doi:10.1029/2011GL048521.

Kistler, R., W. Collins, S. Saha, G. White, J. Woollen, E. Kalnay, M. Chelliah, W. Ebisuzaki, M. Kanamitsu, V. Kousky, H. van den Dool, R. Jenne, and M. Fiorino (2001), The NCEP-NCAR 50-Year Reanalysis: Monthly Means CD-ROM and Documentation, *Bull. Amer. Meteor. Soc.*, *82*(2), 247–267, doi:10.1175/1520-0477(2001)082⟨0247:TNNYRM⟩2.3.CO;2.

Kug, J.-S., and Y.-G. Ham (2011), Are there two types of La Nina?, *Geophys. Res. Lett.*, *38*(16), L16,704, doi:10.1029/2011GL048237.

Kug, J.-S., F.-F. Jin, and S.-I. An (2009), Two Types of El Niño Events: Cold Tongue El Niño and Warm Pool El Niño, *J. Climate*, *22*(6), 1499–1515, doi:10.1175/2008JCLI2624.1.

Lorenz, C., and H. Kunstmann (2012), The hydrological cycle in three state-of-the-art reanalyses: Intercomparison and performance analysis, *J. Hydrometeorol.*, *13*(5), 1397–1420, doi:10.1175/JHM-D-11-088.1.

Neelin, J. D., C. Chou, and H. Su (2003), Tropical drought regions in global warming and El Niño teleconnections, *Geophys. Res. Lett.*, *30*(24), 2275, doi:10.1029/2003GL018625.

Nicholson, S., and J. Selato (2000), The influence of La Niña on African rainfall, *Int. J. Climatol.*, *20*(14), 1761–1776, doi:10.1002/1097-0088(20001130)20:14⟨1761::AID-JOC580⟩3.0.CO;2-W.

Pozo-Vázquez, D., S. R. Gámiz-Fortis, J. Tovar-Pescador, M. J. Esteban-Parra, and Y. Castro-Díez (2005), El Niño–Southern Oscillation events and associated European winter precipitation anomalies, *Int. J. Climatol.*, *25*(1), 17–31, doi:10.1002/joc.1097.

Radebach, A., R. V. Donner, J. Runge, J. F. Donges, and J. Kurths (2013), Disentangling different types of El Niño episodes by evolving climate network analysis, *Phys. Rev. E*, *88*(5), 052,807, doi:10.1103/PhysRevE.88.052807.

Rammig, A., M. Wiedermann, J. F. Donges, F. Babst, W. von Bloh, D. Frank, K. Thonicke, and M. D. Mahecha (2015), Coincidences of climate extremes and anomalous vegetation responses: comparing tree ring patterns to simulated productivity, *Biogeosciences*, *12*(2), 373–385, doi:10.5194/bg-12-373-2015.

Ren, H.-L., and F.-F. Jin (2011), Niño indices for two types of ENSO, *Geophys. Res. Lett.*, *38*(4), L04,704, doi:10.1029/2010GL046031.

Rogers, J. C. (1988), Precipitation Variability over the Caribbean and Tropical Americas Associated with the Southern Oscillation, *J. Climate*, *1*(2), 172–182, doi:10.1175/1520-0442(1988)001⟨0172:PVOTCA⟩2.0.CO;2.

Ropelewski, C. F., and M. S. Halpert (1987), Global and Regional Scale Precipitation Patterns Associated with the El Niño/Southern Oscillation, *Mon. Wea. Rev.*, *115*(8), 1606–1626, doi:10.1175/1520-0493(1987)115⟨1606:GARSPP⟩2.0.CO;2.

Ropelewski, C. F., and M. S. Halpert (1996), Quantifying Southern Oscillation-Precipitation Relationships, *J. Climate*, *9*(5), 1043–1059, doi:10.1175/1520-0442(1996)009⟨1043:QSOPR⟩2.0.CO;2.

Rudolf, B., H. Hauschild, W. Rueth, and U. Schneider (1994), Terrestrial Precipitation Analysis: Operational Method and Required Density of Point Measurements, in *Global Precipitations and Climate Change*, edited by M. Desbois and F. Désalmand, no. 26 in NATO ASI Series, pp. 173–186, Springer Berlin Heidelberg, dOI: 10.1007/978-3-642-79268-7_10.

Schleussner, C.-F., J. F. Donges, R. V. Donner, and H. J. Schellnhuber (2016), Armed-conflict risks enhanced by climate-related disasters in ethnically fractionalized countries, *P. Natl. Acad. Sci.*, *113*(33), 9216–9221, doi:10.1073/pnas.1601611113.

Schneider, U., A. Becker, P. Finger, A. Meyer-Christoffer, B. Rudolf, and M. Ziese (2015), GPCC Full Data Reanalysis Version 7.0 (at 0.5°, 1.0°, 2.5°): Monthly Land-Surface Precipitation from Rain-Gauges built on GTS-based and Historic Data.

Shaman, J., and E. Tziperman (2010), An Atmospheric Teleconnection Linking ENSO and Southwestern European Precipitation, *J. Climate*, *24*(1), 124–139, doi:10.1175/2010JCLI3590.1.

Siegmund, J. F., T. G. M. Sanders, I. Heinrich, E. van der Maaten, S. Simard, G. Helle, and R. V. Donner (2016a), Meteorological Drivers of Extremes in Daily Stem Radius Variations of Beech, Oak, and Pine in Northeastern Germany: An Event Coincidence Analysis, *Front. Plant Sci.*, *7*(733), doi:10.3389/fpls.2016.00733.

Siegmund, J. F., M. Wiedermann, J. Donges, and R. V. Donner (2016b), Impact of temperature and precipitation extremes on the flowering dates of four German wildlife shrub species, *Biogeosciences*, *13*, 5541–5555, doi:10.5194/bg-13-5541-2016.

Siegmund, J. F., N. Siegmund, and R. V. Donner (2017), CoinCalc - A new R package for quantifying simultaneities of event series, *Comput. and Geosci.*, *98*, 64–72, doi:10.1016/j.cageo.2016.10.004.

Taschetto, A. S., and M. H. England (2009), El Niño Modoki Impacts on Australian Rainfall, *J. Climate*, *22*(11), 3167–3174, doi:10.1175/2008JCLI2589.1.

Trenberth, K. E. (1997), The Definition of El Niño, *Bull. Amer. Meteor. Soc.*, *78*(12), 2771–2777, doi:10.1175/1520-0477(1997)078⟨2771:TDOENO⟩2.0.CO;2.

Tsonis, A. A., K. L. Swanson, and P. J. Roebber (2006), What Do Networks Have to Do with Climate?, *Bull. Amer. Meteor. Soc.*, *87*(5), 585–595, doi:10.1175/BAMS-87-5-585.

Wiedermann, M., A. Radebach, J. F. Donges, J. Kurths, and R. V. Donner (2016), A climate network-based index to discriminate different types of El Niño and La Niña, *Geophys. Res. Lett.*, *43*(13), 2016GL069,119, doi:10.1002/2016GL069119.